JASA ARTICLE

Multi-timescale finite element modeling of vocal fold edema progression due to phonotrauma

Jonathan J. Deng,[1] Byron D. Erath,[2] Matías Zañartu,[3] and Sean D. Peterson[1,a)]
[1]*Mechanical and Mechatronics Engineering, University of Waterloo, Waterloo, Ontario N2L 3G1, Canada*
[2]*Department of Mechanical Engineering, Rochester Institute of Technology, Rochester, New York 14623, USA*
[3]*Department of Electronic Engineering, Universidad Técnica Federico Santa María, 2390123 Valparaísa, Chile*

ABSTRACT:
Edema of the vocal folds (VFs) is the result of an inflammatory response to injury (phonotrauma), or other deleterious stimuli, causing fluid build-up in the VF tissue. Although a mild level of edema has been postulated to be prophylactic, excessive edema has been identified as a pathway in the development of vocal hyperfunction. Herein we present a multi-time scale finite element model to examine the progression of VF edema in response to phonotrauma. Phonotraumatic damage was assessed by two measures: viscous dissipation and positive strain energy rate. Time-averaged phonotrauma over short time scales was assumed to drive swelling over longer time scales in proportion to the damage measure via a damage sensitivity gain. Healing was assumed to continuously act to reduce swelling. Growth rate analysis indicated that edema depends on a balance between healing, compensatory adjustments to maintain desired voice output measures, and altered VF vibration due to edema. For high damage sensitivity relative to healing, peak edema resulted in roughly 25% local peak swelling at 0.15 h, whereas low damage sensitivity led to swelling trending toward a steady condition requiring little compensation to maintain voice outputs. In general, fluid accumulation was distributed non-uniformly across the VFs with concentrations near the VF medial surface and the superior end of the body. Results from this first-ever model connecting phonotrauma at the short time scale and swelling at the longer time scale exhibited rapid edema progression under certain conditions, aligned with the "vicious cycle" hypothesis of hyperfunction, wherein localized edema initiated a positive feedback loop that led to even greater localized swelling. https://doi.org/10.1121/10.0042272
(Received 15 April 2025; revised 20 December 2025; accepted 5 January 2026; published online 22 January 2026)
[Editor: Zhaoyan Zhang] Pages: 610–623

I. INTRODUCTION

Edema is the result of an imbalance between fluid influx from capillaries and efflux to the lymphatic system (Gordon Betts *et al.*, 2022) that leads to fluid build-up in the interstitial space. Although many factors may trigger such an imbalance, a common precipitant is the inflammatory response to injury, wherein the wound initiates a complex biochemical response, leading to increased capillary perfusion to the tissue (Mortimer and Levick, 2004). Edema can arise in the vocal folds (VFs) in response to phonotrauma during vibration (Czerwonka *et al.*, 2008), which can negatively impact VF motion and voice outputs (Murphy Estes *et al.*, 2022). Edema has been, for example, correlated with a perception of vocal fatigue (Hunter and Titze, 2009), degradation in voice quality (Bastian *et al.*, 1990), and has been implicated as a potential progenitor of the "vicious cycle" in phonotraumatic vocal hyperfunction (PVH) (Hillman *et al.*, 2020), wherein phonotrauma induces local edema, which is then exacerbated via a positive feedback loop. Furthermore, VF edema likely contributes to variations in the daily phonotrauma index Nudelman *et al.* (2022), an important clinical measure of voice.

As described in a recent scoping review by Watson *et al.* (2024), phonatory loading has been proposed to cause compounded phonotrauma, in which subsequent episodes of tissue injury lead to progressive edema and chronic inflammation extending from the epithelium into the superficial lamina propria. This cascade is theorized to initiate localized pathology via subepithelial fibrovascular changes and increased vascularity to aid tissue healing, potentially culminating in fibrosis rather than complete regenerative repair (Haben, 2012). Verdolini *et al.* (2003) characterized the time course of inflammation-related molecules by swabbing the VFs of a subject after a loud phonation task and found strong shifts in several inflammation-related signals. Other *in vitro* work also shows that human VF fibroblasts respond to pro-inflammatory cytokines and mechanical vibration (Branski *et al.*, 2009; Hortobagyi *et al.*, 2020), consistent with a mechanosensitive inflammatory response on the order of hours (Ingle *et al.*, 2014; Verdolini Abbott *et al.*, 2012). Likewise, acute vocal loading tasks in healthy adults have demonstrated increases in pro-inflammatory cytokines within hours of phonation. These inflammatory cascades are associated with changes in tissue properties, with *in vitro* and *in vivo* studies reporting increased vascular permeability, extracelluluar matrix remodeling (altered collagen and hyaluronan content), and changes in viscoelasticity of the

a)Email: peterson@uwaterloo.ca

https://doi.org/10.1121/10.0042272

lamina propria following phonatory injury or cytokine exposure (Branski *et al.*, 2009; Hortobagyi *et al.*, 2020; Rousseau *et al.*, 2004).

While considerable advances have been made in the exploration of the biological process of edema, the bidirectional connection between VF biomechanics and organ-level inflammatory response remains opaque. Agent-based models and *in vitro* biological studies provide valuable cellular-level information on the progression of the inflammatory process; however, they do not capture the phonatory processes that trigger the inflammation or the resulting change in tissue properties due to inflammation. The latter is particularly important since changes in the tissue's local material properties due to inflammation may influence VF vibration and thus subsequent phonotrauma.

This study aims to develop, for the first time, a model of edema progression, coupling a finite element (FE) model of VF vibration and phonotrauma with a long-time scale model of edema progression and healing. While the molecular mechanisms underlying edema and its progression are not yet fully understood, observations of compounded phonotrauma [see, e.g., Watson *et al.* (2024)] and *in vitro* studies on inflammatory markers [e.g., Hortobagyi *et al.* (2020); Ingle *et al.* (2014); Verdolini Abbott *et al.* (2012)] provide a biologically plausible rationale for representing a slower, tissue-level time scale of injury and healing in our model. Critically, we are interested in the connection between voice use and the rate of VF swelling, toward understanding potentially healthy versus unhealthy VF swelling, with the latter potentially contributing to the "vicious cycle" of phonotraumatic hyperfunction (Hillman *et al.*, 2020). It is hypothesized that coupling between compensatory mechanisms during short voicing time scales and swelling over long tissue time scales affects this rate of VF swelling. To achieve this, we incorporate compensation to maintain the same voice output at each swelling stage and explore conditions that affect the rate of edema progression.

The remainder of the paper is organized as follows: Section II discusses the coupled model used to simulate edema progression. Section III presents simulation results. Section IV discusses the results. Section V clarifies model limitations. Section VI concludes the manuscript.

II. METHODS

The edema progression framework comprises two coupled models bridging disparate time scales. A tissue time scale model (long time scale) captures changes in VF edema in response to the output of a voicing time scale model (short time scale), which provides the measure of phonotrauma driving swelling. We assume that changes in swelling during voicing are negligible; and therefore, the two models can be solved independently, with coupling between the models through source-like terms and tissue property changes (see Fig. 1).

Since edema affects VF geometry and material properties, and therefore voicing, it is expected that individuals will compensate using adjustments of the vocal mechanism to maintain expected voice outputs (Galindo *et al.*, 2017). In general, there are many potentially viable compensatory adjustments (laryngeal musculature adjustments, lung pressure changes, etc.) and voice features [frequency, sound pressure level (SPL), etc.] involved; however, we consider only subglottal pressure compensation to maintain speech volume in this study. Compensation couples the tissue time scale model to the voicing time scale model; specifically, tissue modifications alter the VF dynamics and acoustic outputs, which then necessitate compensatory adjustments to subglottal pressure. We note that the subglottal pressure is treated as constant in the voicing time scale but allowed to vary in the tissue time scale to provide the compensation. Biological observations show that VF tissue swells in response to phonotrauma, both acutely after intense voice use and chronically with repeated loading, linking biomechanical tissue damage to tissue-level inflammatory responses and edema (Branski *et al.*, 2009; Czerwonka *et al.*, 2008; Hortobagyi *et al.*, 2020; Ingle *et al.*, 2014; Leydon *et al.*, 2014; Watson *et al.*, 2024).

A flow chart describing the overarching model and related compensatory action is shown in Fig. 1. The "voicing time scale" model (upper rectangle) captures VF vibration, voice output, and compensatory adjustments to maintain SPL over the voicing time scale, T_v. The "tissue time scale" model (lower rectangle) depicts adjustment to the swelling field (edema), μ, over the tissue time scale, T_t, due to phonotrauma incurred during voicing. Solid arrows indicate general steps involved in solving for the progression of edema; these steps are further described in the respective model sections (see Secs. II A and II B). Coupling between the two models is depicted with dashed arrows.

A. Voicing time scale model

The voicing time scale model consists of a three-dimensional (3D) FE-based model of the VFs coupled with one-dimensional (1D) Bernoulli-based glottal flow models, as shown in Fig. 2. The solid contains a total of 9675 tetrahedral cells split into 15 coronal sections, with each section coupled with a 1D flow model that applies fluid loading to that section.

Tissue kinetics are governed by the conservation of linear momentum. Neglecting body forces this can be written in strong form as follows (Gurtin *et al.*, 2010, their Sec. 19.6):

$$\rho_t \boldsymbol{a} = \nabla \cdot \boldsymbol{\sigma}, \tag{1}$$

where ρ_t is the material density, $\boldsymbol{a}$ is material acceleration, and $\boldsymbol{\sigma}$ is the Cauchy stress tensor. Eq. (1) applies in the current (deformed) configuration of the body. Applying the principle of virtual work and integrating by parts results in the weak form in the current configuration (Gurtin *et al.*, 2010, their Section 22.2) as follows:

$$\int_{\Omega_t} [\rho_t \boldsymbol{a} \cdot \partial \boldsymbol{u} + \boldsymbol{\sigma} : \partial \boldsymbol{\epsilon}] \, \mathrm{d}v - \int_{\partial\Omega_t} p\hat{\boldsymbol{n}} \cdot \partial \boldsymbol{u} \, \mathrm{d}a = 0, \tag{2}$$

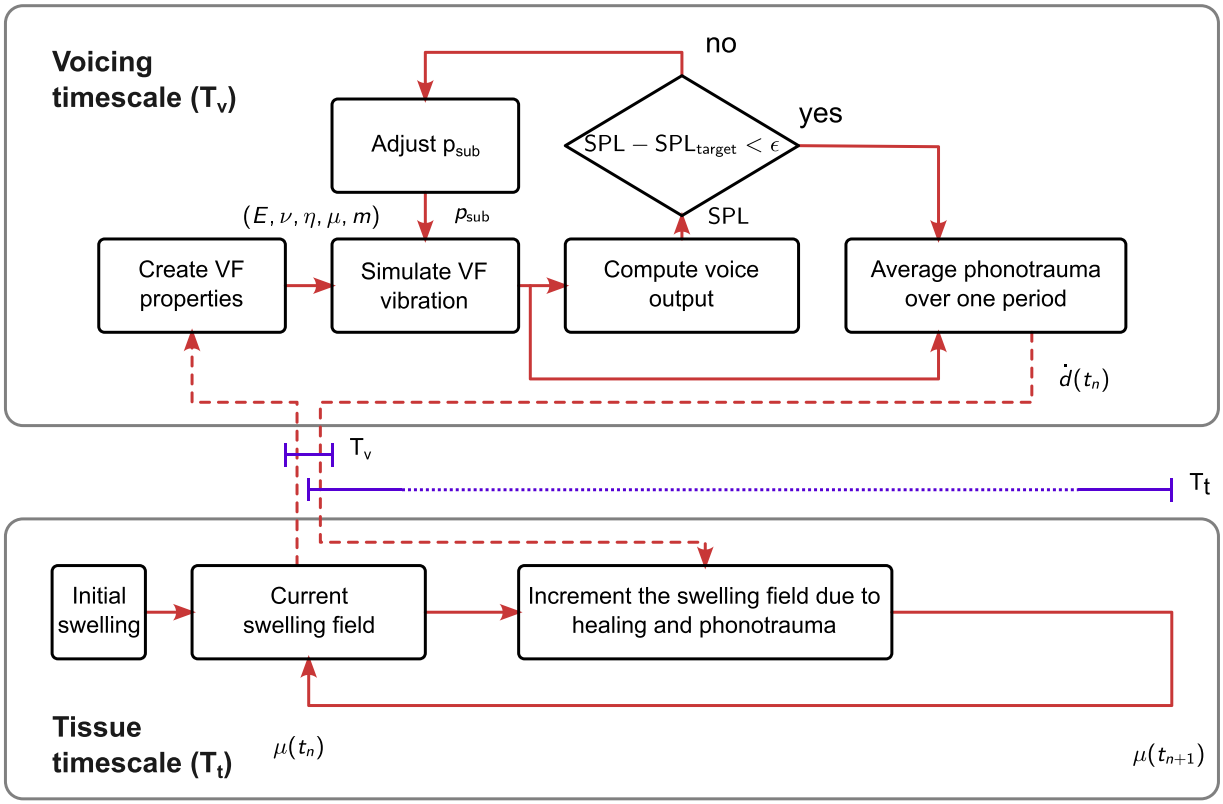

FIG. 1. Flowchart illustrating the coupling between voicing (upper block) and tissue (lower block) time scale models. Dashed arrows indicate coupling data between the two models. Barred lines between the two blocks conceptually illustrate the relative time scales.

where $\partial \boldsymbol{u}$ is the virtual displacement, $\boldsymbol{\epsilon} = 1/2(\boldsymbol{F}^\top + \boldsymbol{F})$ is the infinitesimal strain tensor with $\boldsymbol{F} = \partial \boldsymbol{u}/\partial \boldsymbol{x}$ being the deformation gradient tensor, Ω_t is the deformed VF volume at time t and $\partial\Omega_t$ is its boundary. Aerodynamic loading results in a surface traction $p\hat{\boldsymbol{n}}$, where p is the fluid pressure obtained from the Bernoulli flow model and $\hat{\boldsymbol{n}}$ is a unit vector orthogonal to $\partial\Omega_t$. Mapping Eq. (2) to the reference (undeformed) configuration (Bonet and Wood, 2008; Gurtin *et al.*, 2010, Chapter 8, Chapter 24), Ω (with boundary $\partial\Omega$), results in the Lagrangian formulation as follows:

$$\int_\Omega [\rho \boldsymbol{a} \cdot \partial \boldsymbol{u} + \boldsymbol{S} : \partial \boldsymbol{E}] \, \mathrm{d}v - \int_{\partial\Omega} p \det(\boldsymbol{F}) \boldsymbol{F}^{-\top} \hat{\boldsymbol{n}} \cdot \partial \boldsymbol{u} \, \mathrm{d}a = 0,$$

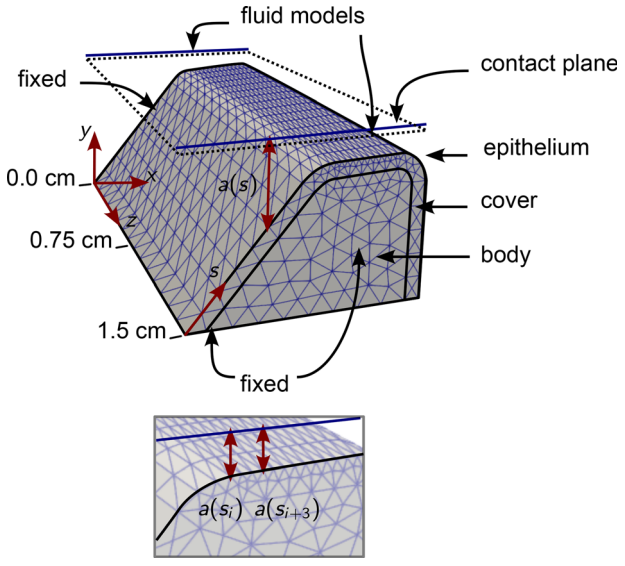

FIG. 2. FE-based VF model schematic showing the M5-based VF geometry (Scherer *et al.*, 2001). The VF interior is divided into cover and body layers with an epithelium membrane at the fluid boundary. Fluid flow is modeled as a collection of independent narrow channels. Inset: Close-up of the fluid model nodes and one-to-one correspondence with nodes on the mesh surface.

where ρ is the reference density, $\boldsymbol{S}$ is the second Piola-Kirchhoff stress tensor, and $\boldsymbol{E}$ is the Green-Lagrange strain tensor. To form our model, we make additional assumptions about viscoelasticity, the constitutive equation for $\boldsymbol{S}$, and the effects of swelling, which results in the governing equation to be solved as follows:

$$\int_\Omega [(1+\mu)\rho \boldsymbol{a} \cdot \partial \boldsymbol{u} + \eta \dot{\boldsymbol{\epsilon}} : \partial \dot{\boldsymbol{\epsilon}} + \boldsymbol{S}(\boldsymbol{E}, e, \nu, \mu, m) : \partial \boldsymbol{E}] \, \mathrm{d}v + \int_{\partial\Omega} \boldsymbol{\sigma}_{\mathrm{epi}} : \partial \boldsymbol{\epsilon}_{\mathrm{epi}} d_{\mathrm{epi}} \, \mathrm{d}a - \int_{\partial\Omega} p \det(\boldsymbol{F}) \boldsymbol{F}^{-\top} \hat{\boldsymbol{n}} \cdot \partial \boldsymbol{u} \, \mathrm{d}a = 0, \quad (3)$$

where $\boldsymbol{v}$ is the material velocity, μ is the swelling field, $(1+\mu)\rho$ accounts for changing density with swelling, η is

https://doi.org/10.1121/10.0042272

the material viscosity, $\boldsymbol{S}(\boldsymbol{E}, e, \nu, \mu, m)$ is the hyperelastic constitutive equation incorporating swelling with (e, ν, μ, m) being material properties (described further below), and $\sigma_{\text{epi}}(e, \nu)\epsilon_{\text{epi}}d_{\text{epi}}$ represents the epithelium membrane (Deng and Peterson, 2023; Deng *et al.*, 2023; Hansbo and Larson, 2014).

The VF constitutive equation was modeled using a Saint-Venant Kirchhoff hyperelastic material with an embedded model of swelling (Deng *et al.*, 2023) as follows:

$$\boldsymbol{S}(\boldsymbol{E}, e, \nu, \mu, m) = \mu^{m+1/3}\left(\frac{e\nu}{(1+\nu)(1-2\nu)}(\operatorname{Tr}\overline{\boldsymbol{E}})\boldsymbol{I} + \frac{e}{1+\nu}\overline{\boldsymbol{E}}\right),$$
$$\overline{\boldsymbol{E}} = \mu^{-2/3}\left(\boldsymbol{E} + \frac{1}{2}(1-\mu^{2/3})\boldsymbol{I}\right), \tag{4}$$

where e is Young's modulus and ν is Poisson's ratio. The swelling modification follows the procedure described in Tsai *et al.* (2004), Pence and Tsai (2005), and Gou and Pence (2016). As mentioned previously, the parameter μ is the local volume change (that is, the swelling field), and m controls the corresponding swelling-induced stiffness changes. If $m > 0$, the material locally stiffens as the local volume increases. Herein a value of $m = -0.8$ was employed based on measured stiffness changes from dehydrating VFs (Yang *et al.*, 2017), with the negative sign indicating material softening with swelling.

The pressure loading, p, was modeled by the 1D Bernoulli equation. Specifically, the fluid domain was divided into 15 coronal sections (Fig. 2), and the flow in each coronal plane was modeled using the 1D Bernoulli equation in order to accommodate for anterior-posterior variations in aerodynamic pressure loading; thus, the flow in each coronal plane is dependent only on the VF geometry in that given plane and is independent of the flow in neighbouring sections. The pressure and flow rate for surface nodes in a given coronal plane are given by the following:

$$p(s) = \begin{cases} p_{\text{sub}} - \dfrac{\rho}{2}q^2 a(s)^{-2}, & s < s_{\text{sep}}, \\ p_{\text{sep}}, & s \geq s_{\text{sep}}, \end{cases} \tag{5}$$

$$q^2 = \frac{2}{\rho}(p_{\text{sub}} - p_{\text{sep}})a(s_{\text{sep}})^2, \tag{6}$$

where p_{sub} is the subglottal pressure, p_{sep} the pressure at the location of flow separation, s is a surface coordinate, and $a(s)$ is the glottal cross-sectional area. As illustrated in the inset of Fig. 2, the Bernoulli model applies pressure to the surface nodes while deformations of the VF change the local cross-sectional area, $a(s)$. Subglottal pressure can be adjusted as a compensatory action (see Sec. II A 2; Fig. 1). Flow separation was specified at s_{sep}, defined as when $a(s)/a_{\min} > 1.2$ (Decker and Thomson, 2007; Geng *et al.*, 2021).

Numerical solution of Eq. (3) was conducted using a simulation code written in Python, which used the FE framework FEniCS (Logg and Wells, 2010) and scientific Python packages including NumPy (Harris *et al.*, 2020) and SciPy (Virtanen *et al.*, 2020). All codes have been made available via a GitHub repository (https://github.com/jon-deng/vf-swelling). Equation (3) was integrated in time using the Newmark time stepping scheme (Newmark, 1962) to approximate acceleration, $\boldsymbol{a}$, and velocity, $\boldsymbol{v}$, as functions of displacement, $\boldsymbol{u}$, over a period of $T = 0.4096$ s with a time step of $\Delta t = 5 \times 10^{-5}$ s. At each time step, this involves solving the Newmark discretized weak form over the entire domain in Fig. 2. Contact was modeled by enforcing a minimum gap between the VFs with a penalty pressure in addition to Bernoulli fluid pressure. Material properties were allowed to vary element to element due to swelling, as well as from layer to layer in the VFs. Integrating the voicing model over T therefore results in a time-history of VF acceleration, velocity, and displacement states $(\boldsymbol{a}, \boldsymbol{v}, \boldsymbol{u})$ and glottal flow and pressure states (p, q).

A summary of constant parameter values employed in the voicing time scale simulations, as well as the references from which they were obtained, is given in Table I.

1. Measures of phonotrauma

The biological mechanisms underlying VF edema progression in response to phonotrauma are complex and yet to be fully understood (Johns, 2003; Verdolini *et al.*, 2003). From the modeling standpoint, a critical element that remains obscure is what mechanical measures best represent phonotrauma and how they relate to an inflammatory tissue response. Herein we consider viscous dissipation and strain energy rate as candidate measures of phonotrauma leading to edema. Viscous dissipation was introduced by Titze and Hunter (2015) in the form of a dissipated energy dose and further explored by Motie-Shirazi *et al.* (2021), whereas strain energy is often employed by the continuum damage mechanics community (see, e.g., Balzani *et al.*, 2012;

TABLE I. Constant parameter values. References from which the values were obtained are provided in the right-most column.

Parameter	Value	References
e_{body}	5.0 kPa	1–3
e_{cover}	2.5 kPa	1–3
e_{epi}	50 kPa	4, 5
η	0.5 Pa s	1
ν	0.4	
m	−0.8	6, 7
d_{epi}	0.005 cm	4, 5
p_{sub}	400 Pa (nominal)	
T	0.4096 s	
Δt	5×10^{-5} s	

[1]Alipour-Haghighi *et al.* (2000).
[2]Murray and Thomson (2011).
[3]Miri (2014).
[4]Hirano *et al.* (1982).
[5]Hirano and Kakita (1985).
[6]Yang *et al.* (2017).
[7]Deng *et al.* (2023).

Chaboche, 1988). In the present study, viscous dissipation is computed as follows:

$$\dot{d} = \eta \dot{\boldsymbol{\epsilon}} : \dot{\boldsymbol{\epsilon}}, \tag{7}$$

and positive strain energy rate as follows:

$$\dot{d} = \lfloor \boldsymbol{S}(\boldsymbol{E}, e, \nu, \mu, m) : \dot{\boldsymbol{E}} \rfloor, \tag{8}$$

where $\lfloor \cdot \rfloor$ denotes the positive part of the strain energy rate (all negative strain energy rates become 0).

These damage measures vary in time due to VF vibration. The time-averaged damage rate at a given point in the VFs, which is assumed to correlate with edema growth, is computed by integrating Eq. (7) or Eq. (8) over the voicing period. Only the latter half of the voicing period ($T = 0.4096$ s) is considered when computing the average phonotrauma to avoid contamination by numerical transients.

2. Compensatory adjustments and voice outputs

A simplified compensatory adjustment model is employed, wherein only subglottal pressure, p_{sub}, changes to maintain a target SPL. While in reality, there are multiple compensatory mechanisms and compensatory targets, we restrict our consideration to a single parameter for simplicity of demonstration. Previous observations have shown that subglottal pressure is the dominant factor affecting SPL (Chhetri and Park, 2016; Galindo *et al.*, 2017).

SPL is computed as the radiated pressure using the piston-in-baffle approximation (Kinsler *et al.*, 2000) for the glottal flow rate, q, as follows:

$$\hat{p}_{\text{rad}} = \frac{j}{2\pi r} \rho c \hat{q} k \exp(jkr), \tag{9}$$

where $r = 1$ m is the distance from the source, $c = 340\ \text{m s}^{-1}$ is the speed of sound, and $j = \sqrt{-1}$. The variables $\hat{q}$ and $\hat{p}_{\text{rad}}$ are complex Fourier-components of the flow rate and pressure waveform, respectively, and $k = f/c$ is the corresponding wavenumber. The flow rate waveform was computed as the total flow rate from each coronal plane. SPL, denoted as L_{p}, was then computed according to the following:

$$L_{\text{p}} = 20 \log_{10} \frac{\frac{1}{n} \sum_{i=0}^{n-1} ||\hat{p_{\text{rad}}}^{i}||^2}{20\ \mu\text{Pa}}, \tag{10}$$

where $\hat{p}^{i}_{\text{rad}}$ is the ith Fourier component of the radiated pressure. Compensatory adjustments were computed by employing a Newton-Raphson procedure that iteratively adjusted p_{sub} for a given VF configuration model until its output SPL matched that of the nominally unswollen VF.

B. Tissue time scale model

The tissue time scale model captures phonotrauma-induced increases and healing-induced reductions in edema according to the following:

$$\dot{\mu} = K \dot{d}(t) - H\mu, \tag{11}$$

where μ depends on position within the VF, $\dot{d}(t)$ is the phonotrauma rate from the voicing-time scale model, and K and H are gains representing phonotrauma and healing, respectively (further described below). Note that Eq. (11) and the voicing time scale equations [Eq. (3)] represent a coupled set of ordinary differential equations governing the simultaneous evolution of edema and VF vibrations.

Tissue changes occur over vastly longer times than VF vibrations; as such, the coupled tissue and voicing time scale models cannot be efficiently solved together for long durations. To address this, we aim to predict the tissue-time scale dynamics by decoupling the two time scales using an approach inspired by homogenization and multiscale modeling techniques (Pavliotis and Stuart, 2008, their Chap. 8). Consider the voicing time scale, T_{v} (the time of a single voicing period) and the tissue time scale, T_{t}, where $T_{\text{t}} \gg T_{\text{v}}$. While the instantaneous damage rate will vary due to VF oscillations over the time scale T_{v}, we hypothesize the time-averaged damage rate over limit cycles of the VF vibration will vary over a much longer time $T_{\text{v}} \ll \Delta t \ll T_{\text{t}}$. The periodic behavior may in turn slowly change as tissue properties changeover the tissue time scale, T_{t}. The period-averaged damage rate is given by the following:

$$\overline{\dot{d}}(p_{\text{sub}}(\mu), \mu) = \frac{1}{T} \int_{t_0}^{t_0+T} \dot{d}(t) \mathrm{d}t,$$

where t_0 is an arbitrary starting time and T is the limit cycle period. The dependence of $\overline{\dot{d}}$ on μ represents how edema changes tissue kinetics, whereas the dependence on p_{sub} encapsulates compensatory adjustments. For time steps $T_{\text{v}} \ll \Delta t \ll T_{\text{t}}$ the increment in edema is then

$$\begin{aligned} \Delta\mu &= \int_{t_0}^{t_0+\Delta t} \left(K\dot{d}(t) - H\mu(t)\right) \mathrm{d}t \\ &\approx \left(K\overline{\dot{d}}(p_{\text{sub}}(\mu), \mu) - H\mu(t)\right) \Delta t. \end{aligned}$$

Therefore, we expect the period-averaged phonotrauma effectively acts as the damage rate for times $T_{\text{v}} \ll \Delta t \ll T_{\text{t}}$ and approximate the decoupled tissue-time scale dynamics by the following:

$$\dot{\mu} = K\overline{\dot{d}}(p_{\text{sub}}(\mu), \mu) - H\mu. \tag{12}$$

We numerically approximate this by integrating voicing time scales over the last half of the simulation period.

Direct experimental measurements of the short-term decay of interstitial edema in human VFs are scarce. However, behavioral and perceptual studies of vocal fatigue and recovery following vocal loading show recovery trajectories that are well approximated by exponential-like decay with characteristic recovery on the order of hours, motivating the use of an exponential term, $H\mu$, in Eq. (12) to represent short-term resorption of edema and recovery of vocal

https://doi.org/10.1121/10.0042272

effort at the tissue time scale (Hunter and Titze, 2009). *In vitro* experiments on mechanically stimulated VF fibroblasts further demonstrate that mechanical loading modulates inflammatory signaling, supporting the idea that the effective decay rate of acute edema will depend on phonatory loading history and mechanotransduction (Hortobagyi *et al.*, 2020). Thus, the exponential decay used here is a pragmatic representation of short-term (in the tissue time scale) edema resolution. Specifically, we employ $H = -\log(0.5)/5\,\mathrm{h}$ for our model, which we extract from vocal fatigue observations from Hunter and Titze (2009).

C. Edema growth rate of the tissue time scale model

In Eq. (12), $\bar{\dot{d}}$ is the time-averaged rate of phonotrauma during voicing from integrating either Eq. (7) or Eq. (8) over the voicing period, see Sec. II A. Thus, the damage sensitivity (K) represents the bulk effect of sensitivity of swelling to the chosen damage measure, as well as a duty cycle accounting for intermittent voicing over long periods of time. While the percent of time spent voicing can be quantified, the biological sensitivity of edema to a mechanical damage measure remains elusive. The relationship between tissue damage and edema is complex with little quantitative supporting data; as such, we restrict our model to the use of a simple gain K.

To determine reasonable values for K, we consider a growth rate analysis of Eq. (12) to find values of K that result in "fast" and "slow" edema progression. Specifically, we linearize Eq. (12) about the unswollen state, $\mu = 1$, yielding a linearized model of the following form:

$$\dot{\Delta\mu} \approx \Lambda\Delta\mu + K\bar{\dot{d}}|_{\mu=1}, \tag{13}$$

$$\Lambda = \left(K\frac{\partial\bar{\dot{d}}}{\partial\mu} + K\frac{\partial\bar{\dot{d}}}{\partial p_{\mathrm{sub}}}\frac{\partial p_{\mathrm{sub}}}{\partial\mu} - H\boldsymbol{I}\right), \tag{14}$$

where $\Delta\mu = \mu - 1$, $\Lambda = \mathrm{d}\bar{\dot{d}}(p_{\mathrm{sub}}(\mu),\mu)/\mathrm{d}\mu$ is a matrix representing the growth rate of the edema field with time (since $\bar{\dot{d}}$ and μ are both scalar fields), and $\boldsymbol{I}$ is the identity matrix. We note that this differs from a traditional stability analysis wherein an equilibrium edema state would be found, and then the stability about that state would be evaluated. We elect to linearize about $\mu = 1$ to limit computational cost.

The growth rate, Λ, can be decomposed into a set of edema growth modes (eigenvectors) and corresponding growth rates (eigenvalues). Modes with positive eigenvalues represent edema distributions that grow exponentially with time, whereas those with negative eigenvalues decay exponentially with time. This eigenvalue decomposition of Λ is computationally expensive ($\bar{\dot{d}}$ requires integrating the voicing time scale model); as such, we opt to approximate it based on the growth rate of an *a priori* selected edema distribution, $b\Delta\mu^*$, where $\Delta\mu^*$ is the unit edema distribution ($\Delta\mu^{*\top}\Delta\mu^* = 1$), and b its magnitude. This results in the following:

$$\dot{\Delta\mu} \approx \Lambda\Delta\mu^* b + K\bar{\dot{d}}|_{\mu=1}.$$

Assuming the magnitude is given by $b = \Delta\mu^{*\top}\Delta\mu$ for any edema distribution, $\Delta\mu$, the linearized edema magnitude is governed by the following:

$$\begin{aligned}\dot{b} &= \Delta\mu^{*\top}\dot{\Delta\mu} \approx \Delta\mu^{*\top}\Lambda\Delta\mu^* b + \Delta\mu^{*\top}K\bar{\dot{d}}|_{\mu=1}\\ &\approx \lambda b + \Delta\mu^{*\top}K\bar{\dot{d}}|_{\mu=1}.\end{aligned} \tag{15}$$

The growth rate of the selected edema distribution's magnitude, b, is then given by the scalar:

$$\begin{aligned}\lambda = \Delta\mu^{*\top}\Lambda\Delta\mu^* &= K\Delta\mu^{*\top}\frac{\partial\bar{\dot{d}}}{\partial\mu}\Delta\mu^*\\ &+ K\Delta\mu^{*\top}\frac{\partial\bar{\dot{d}}}{\partial p_{\mathrm{sub}}}\frac{\partial p_{\mathrm{sub}}}{\partial\mu}\Delta\mu^*\\ &- H\Delta\mu^{*\top}\Delta\mu^*.\end{aligned} \tag{16}$$

To distinguish between "high" and "low" K values, we determine a critical value, K_{c}, for zero growth rate, $\lambda = 0\,\mathrm{h}^{-1}$, given by the following:

$$K_{\mathrm{c}} = H\left(\Delta\mu^{*\top}\frac{\partial\bar{\dot{d}}}{\partial\mu}\Delta\mu^* + \Delta\mu^{*\top}\frac{\partial\bar{\dot{d}}}{\partial p_{\mathrm{sub}}}\frac{\partial p_{\mathrm{sub}}}{\partial\mu}\Delta\mu^*\right)^{-1}. \tag{17}$$

Numerical values of K_{c} are computed from Eq. (17) by replacing the derivative terms with finite-difference approximations. To find "fast" growth rates, we picked K such that $\lambda = 1\,\mathrm{h}^{-1}$ for each damage measure, whereas to find "slow" growth rates, we picked K such that $\lambda = -0.1\,\mathrm{h}^{-1}$. Neglecting the non-homogeneous term, the first-order linear ordinary differential equation in Eq. (16) suggests that the edema magnitude evolves according to $b(t) \approx \exp(\lambda t)$. This suggests for initial small changes in swelling, the fast growth rate corresponds to tripling the swelling magnitude every hour while the slow growth rate decreases swelling by 10% each hour. The resulting edema growth rates and damage sensitivities, K, are provided in Table II.

III. RESULTS

In this section, we elect to present results for high K ("fast" growth) with viscous dissipation as the damage measure (Sec. III A) to highlight general features of edema evolution. Differences observed with strain rate energy as the

TABLE II. Summary of simulation cases.

Damage measure	Growth rate	K (cm^3/erg)
Viscous dissipation	fast	1.2×10^{-5}
Viscous dissipation	slow	4.1×10^{-7}
Strain energy rate	fast	1.5×10^{-8}
Strain energy rate	slow	5.2×10^{-10}

damage measure and for varying K are presented in Sec. III B.

A. Viscous dissipation: "Fast" edema growth rate

Figure 3 shows the progression of edema states at key time steps. Edema is initially minimal but increases non-homogeneously with time. It is greatest at the mid-coronal medial surface, which corresponds to the VF collision zone. Edema is more broadly distributed within the body layer, although there is a concentrated region toward the superior margin near the where the VF connects to the rigid basement membrane. It is likely that this is in part an artifact of the applied rigid boundary condition and sharp corner leading to a high stress concentration. The local volume growth reaches nearly 20% at these concentrated locations, illustrating the potential for non-homogeneous edema growth in the VFs.

Figure 4 presents the corresponding compensatory subglottal pressure. As edema increases, compensatory subglottal pressure clearly increases in order to maintain the same SPL with the new swollen VF configuration. Although potentially counter-intuitive, we have previously shown that swelling results in several changes to the VFs that influence their dynamics, including decreasing stiffness, increasing mass and volume, and altering the pre-phonatory gap (Deng *et al.*, 2023). Increasing mass and decreasing pre-phonatory gap tend to reduce SPL, with the latter likely being the predominant effect here. The corresponding average degree of swelling is presented in Fig. 5(a), which shows that, whereas subglottal pressure growth rate increases with tissue time, the average level of edema exhibits roughly linear growth with only very modest evidence of slowing, aligned with the linearized growth rate analysis of Sec. II C. The total volume change in the body slightly exceeds that of the cover, but both reach around 2% after 0.15 h of tissue time. Conversely, a compensatory subglottal pressure increase in approximately 25% is observed by 0.15 h. As suggested by the last row of Fig. 3, local tissue swelling can far exceed the average value.

Figure 5(b) shows the volume change at the two locations in the coronal mid-plane, identified in Fig. 3, corresponding to locations of high localized swelling. At these points, swelling increases approximately linearly with time, mimicking the qualitative trend in average edema seen in Fig. 5(a). Figure 5(c) quantitatively illustrates the non-uniformity in

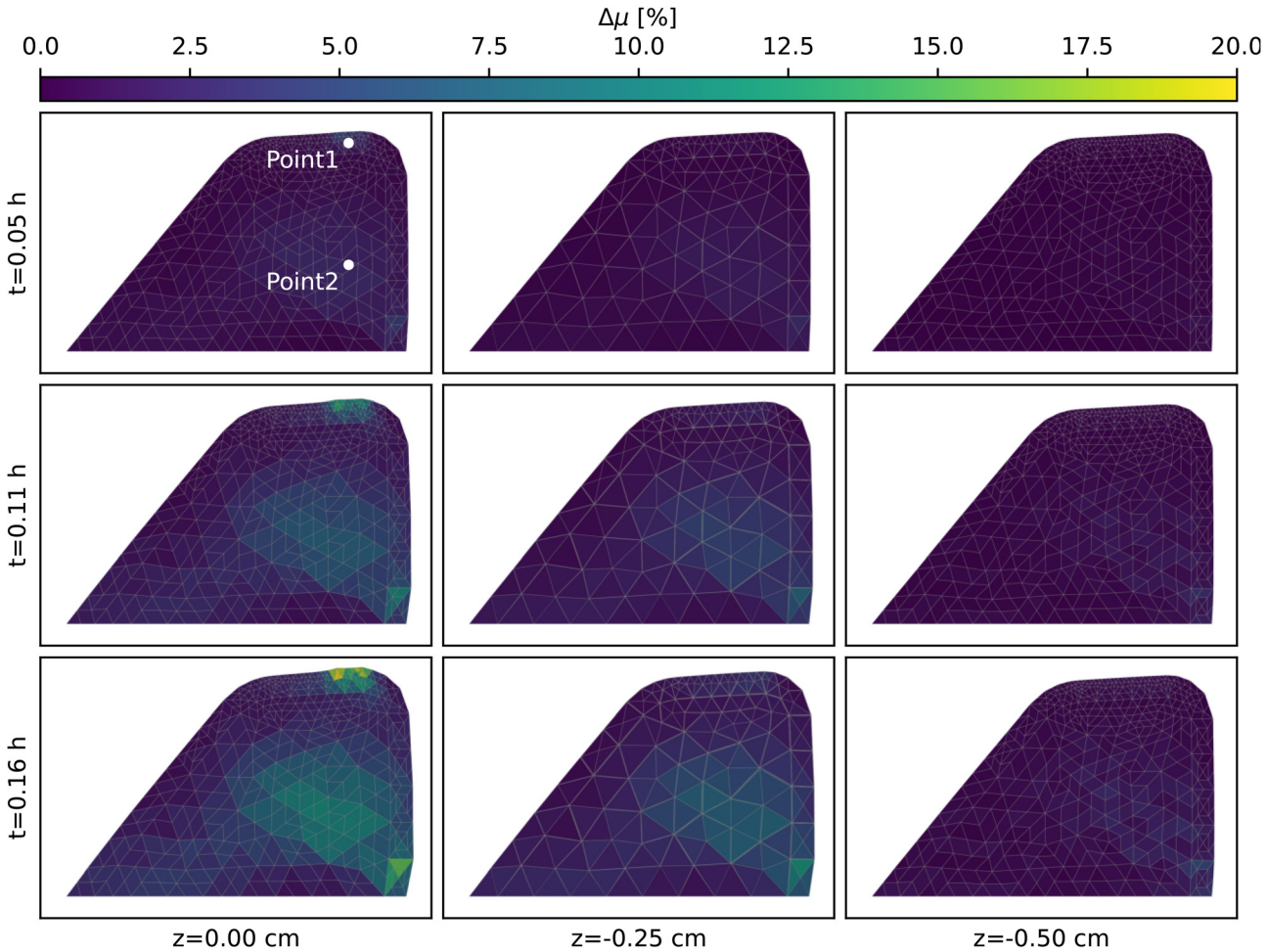

FIG. 3. Progression of swelling states with time (rows from top to bottom) and moving away from the mid-coronal plane (columns from left to right). Swelling progression is based on the viscous dissipation damage measure.

https://doi.org/10.1121/10.0042272

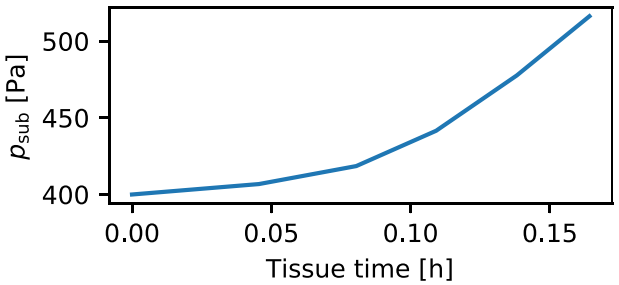

FIG. 4. Compensatory subglottal pressure with phonation time. The compensatory subglottal pressure increases with time to maintain a constant SPL, which would otherwise decrease due to increasing edema.

edema; for example, at 0.15 h, just 10% of the VF volume experiences more than 5% swelling, further demonstrating the highly localized nature that damage-induced swelling can exhibit.

Figure 6 presents the displacement of the medial surface along the coronal plane due to swelling over time. In the collision region (highlighted in gray), the VF swells outward by about 0.02 cm over the course of 0.15 h in comparison to the unswollen condition at 0 h. The entire medial surface displaces due in part to swelling within the body layer. A small bump is also seen to be forming at 0.16 h.

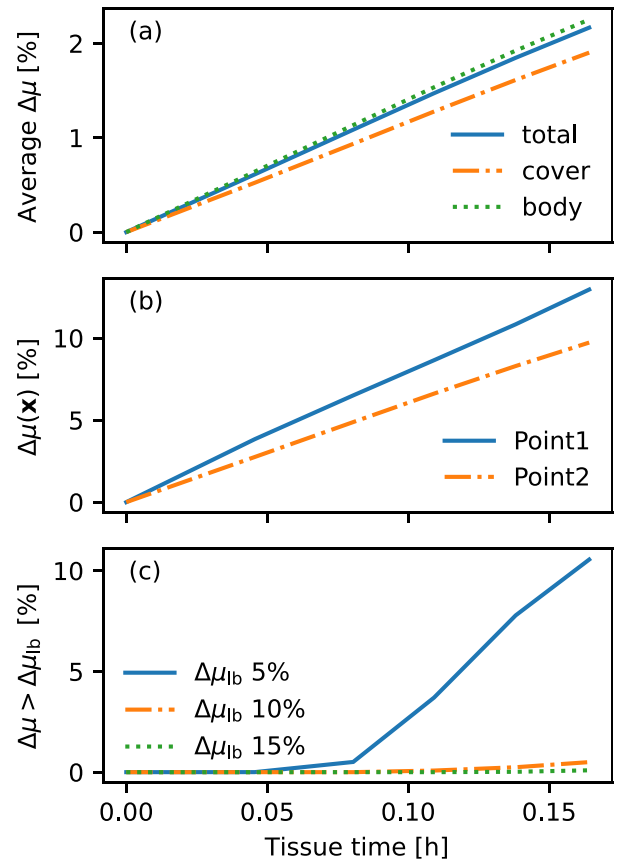

FIG. 5. (a) The average change in volume due to swelling as a function of tissue time, (b) the volume change at two locations in the coronal midplane (see Fig. 3), and (c) the fraction of VF volume that exceeds a threshold swelling, $\Delta\mu_{1b}$.

Figure 7 shows the time-averaged glottal flow rate and closed quotient on the tissue time scale. Qualitatively, the flow rate waveforms on the voicing time scale are essentially sinusoidal for all levels of swelling (tissue time instances), so they are excluded for brevity. While the coronal midplane flow rate clearly decreases as edema progresses (except past 0.15 h), the anterior-posterior (AP) averaged flow rate begins increasing at 0.08 h. This is likely due to the effect of the edema bump at the coronal midplane. As the bump grows, the midplane area decreases; however, during contact, the bump prevents full closure around the bump geometry, thus increasing leakage flow and the AP averaged flow rate. The closed quotient increases as the VFs swell due to the localized swelling at the medial surface, which decreases the gap between the VFs in the resting state.

B. Effects of edema damage sensitivity and damage measure

The edema damage sensitivity, K, affects how quickly edema grows with time. Figure 8 shows the compensatory subglottal pressure and average volume change for "slow" edema growth (small K) based on viscous dissipation. There are clear differences in the compensatory subglottal pressure and average swelling compared to the "fast" growth (high K) seen in Figs. 4 and 5. The average volume change appears to slow as tissue time progresses, and comparable amounts of swelling take longer times to achieve. Compensatory subglottal pressure grows during this time but at a significantly slower rate compared to the "fast" edema growth case.

The choice of damage measure also impacts edema growth through changes in the swelling distributions. Figure 9 shows the edema states with time for varying coronal planes using positive strain energy rate as the damage measure. Similar to the edema distributions based on viscous dissipation seen in Fig. 3, edema is distributed non-uniformly and concentrated near the medial surface and within the body layer of the VF, albeit with minor differences due to the different damage measure. For example, at the superior margin, viscous dissipation-based edema is locally concentrated in the cover

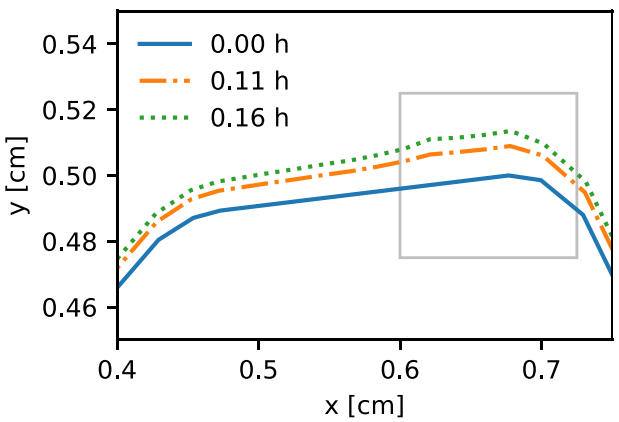

FIG. 6. Medial surface displacement in the mid-coronal plane ($z = 0.0$ cm) with time. The gray box highlights the approximate collision region.

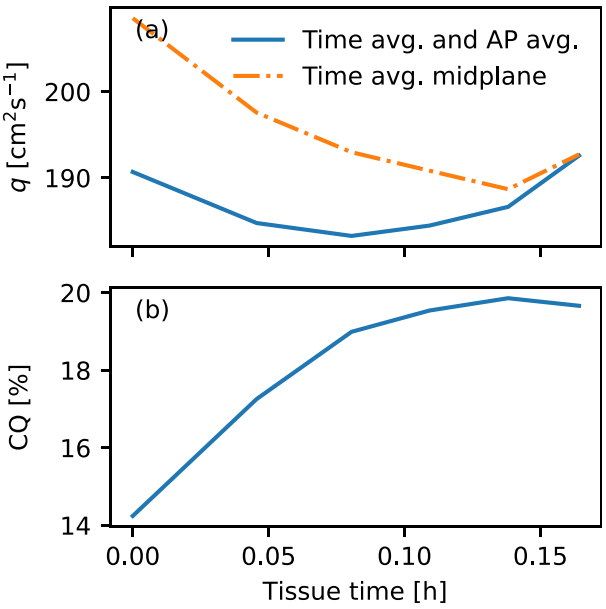

FIG. 7. (a) Time-averaged glottal flow rate for the coronal midplane and for the average over all coronal planes and (b) corresponding closed quotients (for the midplane). Closed quotients are computed for the coronal-midplane flow waveform.

layer, while strain energy rate-based edema is locally concentrated in the body layer. Roughly speaking, viscous dissipation is large wherever viscosity (uniform in our case) is high and strain rates are large [Eq. (7)], whereas strain energy rate is large wherever stresses and strain rates are large [Eq. (8)]. Near the superior margin, the disparate body and cover stiffnesses result in unequal loading carried by the two layers, which thus localizes the majority of the strain energy rate in the body. In contrast, uniform viscosity results in a concentration of viscous dissipation within the cover layer instead.

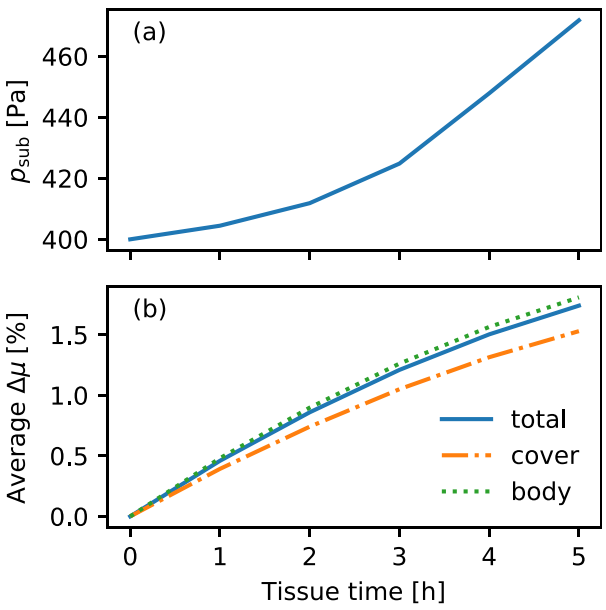

FIG. 8. (a) Compensatory subglottal pressure and (b) change in volume due to swelling as function of tissue time.

Despite these differences, similar peak edema magnitudes are present at comparable times; for example, the peak volume increase is about 18% at 0.37 h for strain energy rate-based edema (Fig. 9) and about 20% at 0.16 h for viscous dissipation-based edema (Fig. 3). Similarly, we found only slight differences in the resulting trends in volume growth, the results of which are omitted for brevity.

IV. DISCUSSION

The growth rate analysis in Sec. II C (Eq. (16) decomposes the swelling growth rate into three effects: edema growth due to altered dynamics from edema, edema growth due to compensatory actions from edema, and edema reduction due to healing. The first two mentioned factors are also affected by the base VF properties (e.g., viscosity and stiffness), which illustrates how individual biomechanical differences can affect edema progression. For example, a propitious combination of VF layer properties or low VF viscosity for an individual may allow them to produce large SPL changes with low subglottal pressure changes which would reduce the effect of edema growth due to compensatory adjustments. *In vitro* bioreactor experiments have demonstrated that mechanical stimulation in the form of model vibrational stress actually promotes anti-inflammatory factors in VF tissue in an inflammatory state (Hortobagyi *et al.*, 2020), supporting the inclusion of a healing factor in our model. Healing was modeled assuming exponential behavior with its rate governed by the parameter H. For a given sensitivity to phonotrauma (fixed K), were the healing response more pronounced (higher H), the progression of edema would be slowed. We note that healing in our model is relegated to the tissue time scale and does not directly influence voicing time scale kinetics.

The growth rate analysis (Sec. II C) also suggests factors that affect the progression of edema. First, the proportionality from phonotrauma to edema and the phonation duty cycle, captured in K, affect edema growth. The greater the biological sensitivity of swelling to phonotrauma or the more time an individual spends talking, the greater the value of K and the more rapidly edema progresses. Second, the model suggests that individuals who require high subglottal pressures to speak louder will experience faster swelling growth. Third, the model shows the importance of healing in the swelling response. Individuals with strong healing responses would experience less rapid edema growth. Should an individual reduce the amount of time speaking, such that K decreases further (e.g., to zero), then healing would ultimately cause edema to reduce.

The non-homogeneous edema distribution (Figs. 3 and 9) has important impacts on the progression of edema. Due to the concentration of damage measures at the medial surface, swelling is also concentrated there, and results in the formation of a localized bump (Fig. 6). For the degrees of swelling seen in our study, this did not significantly impact phonation characteristics after compensatory subglottal pressure changes, for example, in terms of flow

https://doi.org/10.1121/10.0042272

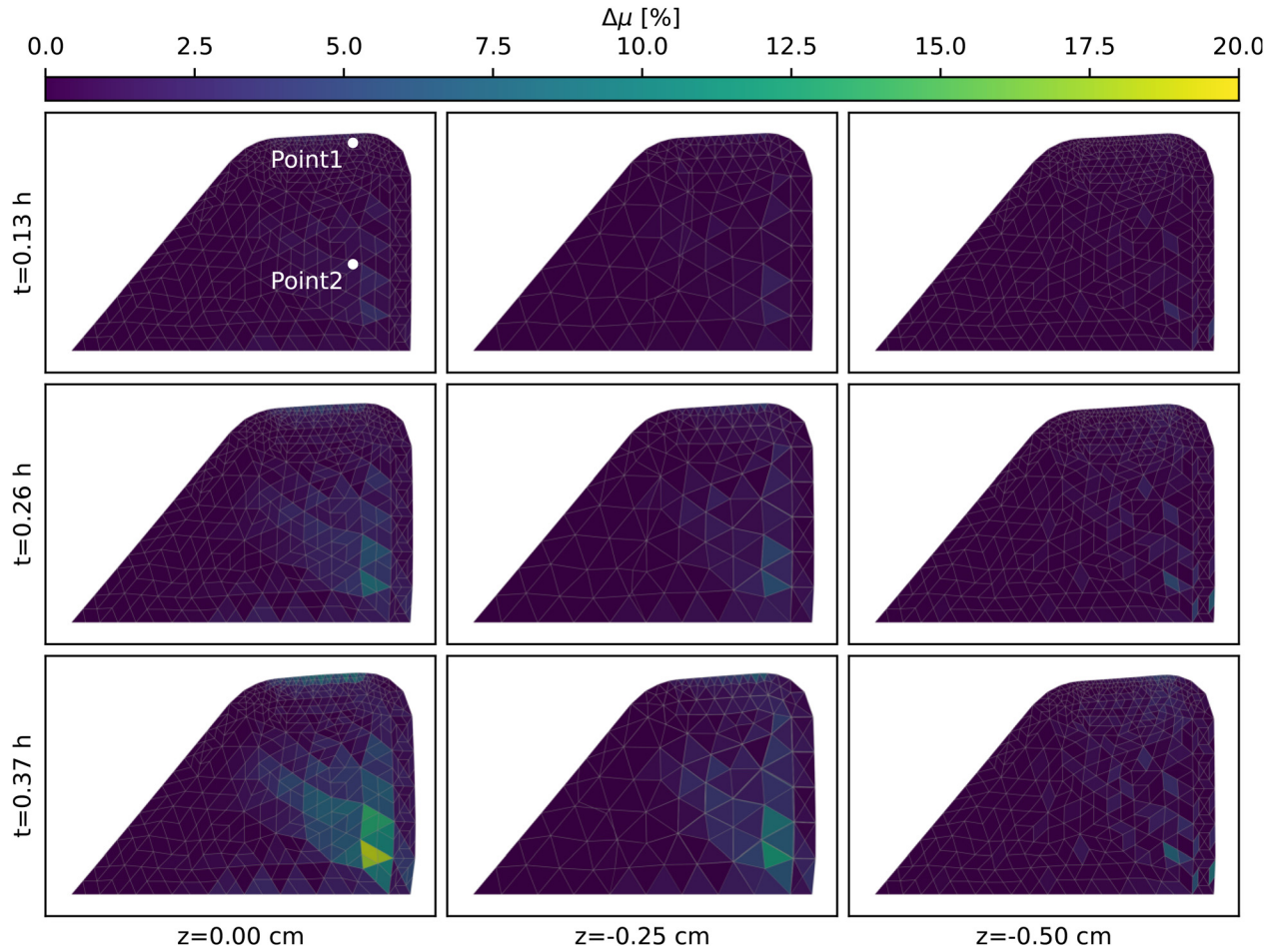

FIG. 9. Progression of swelling states with time (rows from top to bottom) and moving away from the mid-coronal plane (columns from left to right). Swelling progression is based on the positive strain energy rate damage measure. See Fig. 2 for the coronal plane locations.

waveforms and closed quotient (Fig. 7). With further edema progression, these localized bumps could significantly disturb glottal airflow and potentially develop into phonotraumatic lesions. The distribution of swelling also depends on the measure of phonotrauma used; the two measures of phonotrauma developed qualitatively similar distributions albeit with different localized swelling rates. As previously mentioned, we suspect that the swelling concentration in the body is a product of the problem setup and not physiologically meaningful. That said, although its effect on edema progression is less clear, it generally results in a slight outward expansion of the VF surface. Future work will refine the model geometry to better represent the connection of the VFs to the basement membrane.

The PVH "vicious cycle" (Hillman *et al.*, 2020; Holmberg *et al.*, 2003) is a hypothesis on the etiology of phonotraumatic lesions, such as nodules. Our results support this hypothesis by showing that, for some conditions, compensatory subglottal pressure increases are self-reinforcing and lead to edema growth. The fact this does not always happen also agrees with clinical observations of phonotraumatic lesion development; while swelling happens for all individuals, not everyone develops phonotraumatic lesions. Individual biomechanical differences would affect how individuals compensate for edema and how edema alters their VF dynamics, ultimately presenting as differences in the progression of edema. For example, the model demonstrates the important balance between damage sensitivity, K, and the healing rate, H. Individuals with comparatively weak healing responses would be more prone to developing PVH.

The results also agree with findings on VF nodule locations and their effects on voicing. A number of previous studies focusing on mechanical measures (stress, pressure, etc.) (Czerwonka *et al.*, 2008; Gunter, 2004; Jiang and Titze, 1994; Tao and Jiang, 2007) all found peaks midway along the AP axis of the VFs, which is where lesions are clinically observed. The two different mechanical measures investigated in our study also agree with this and show that swelling, which could develop into nodules, forms midway along the AP axis. In terms of voicing effects, Jiang *et al.* (2004) found subjects with VF nodules had reduced vocal efficiency compared to subjects without when asked to perform phonation tasks at set target volumes (soft, medium, and loud phonation). Our results agree with this, predicting that compensatory increases in subglottal pressure are required as an edema bump grows, which roughly resembles a nodule shape, and that the edema also tends to increase the

average glottal flow rate, thus resulting in increased input aeroacoustic power (effort) for the same loudness condition. In a similar study, Zhuang *et al*. (2009) found that phonation threshold flow was increased in individuals with nodules or polyps compared to those without. This was corroborated by silicone VF studies which found similarly increasing phonation threshold pressure and flow with increasing nodule or polyp diameter (Motie-Shirazi *et al*., 2023). Our results agree with these findings since they suggest that achieving the same loudness with a medial surface bump requires larger subglottal pressures and glottal flow rates.

V. LIMITATIONS

There are several important limitations of our model and its predictions, which we separate into subsections of foundational biological data and computational modeling below.

A. Limited biological data

The paucity of biological data upon which to ground our model parameters is the most significant limitation of this study. This results in two important sources of uncertainty in our model: how to choose the best mechanical measure of damage that drives edema and how to model the sensitivity of edema to that damage (captured in K). To address the former, we elected to explore two candidate measures: viscous dissipation, which has precedent as a "dissipated-energy dose" metric for phonation (Hunter and Titze, 2009), and positive strain-energy rate, a common measure in continuum damage mechanics. While these provide plausible proxies, additional biological insights, such as single-cell and gene-expression experiments, are needed to identify and validate appropriate damage measures. To address the latter, we chose K values to represent distinct ends of the spectrum (Sec. II C), one showing very rapid swelling (with the rate tripling over an hour), as would be expected in response to acute trauma, and the other a much slower seeping of fluid into the region, typically of inflammation via repetitive use. This is not to imply that the particular values of K are derived from biological data, which is scarce as best, or even necessarily represent any specific case, but rather to exemplify qualitatively plausible behaviors. Furthermore, it is likely that damage sensitivity and healing rates depend on the tissue and the type of mechanical loading/damage experienced. That is, it is reasonable to assume that values of K and H would differ between layers of the folds, which we neglected in this initial model offering. Strengthening the connection between biological evidence and biomechanical modeling remains an important direction for future work.

The use of an exponential decay term for edema resolution and a simple load-dependent gain parameter in our healing model are pragmatic simplifications. While these choices are supported by vocal recovery trajectories and *in vitro* fibroblast studies showing mechanosensitive inflammatory responses (Hortobagyi *et al*., 2020), direct measurements of edema kinetics *in vivo* and the longer-term ECM remodeling processes are not represented in this model.

We further note that the data from which we compiled our model parameters (see Table I) rely on a range of study types, not all of which have consistent data collection protocols and/or modeling assumptions. As such, there is a level of uncertainty in these modeling parameters and selection of alternate values may change the details of the present model predictions. Significant alterations to model trends are not anticipated, however.

At the present state, due to limited biological data available to ground model parameters, model outputs are more phenomenological than predictive, illustrating possible trajectories for swelling based upon the balance between damage sensitivity and healing. However, the model does demonstrate how healing, damage, and compensatory responses can couple across disparate time scales to result in different swelling growth trajectories. Moreover, the demonstrated "fast" and "slow" progression trajectories align with hypotheses of swelling pathways toward the vicious cycle in hyperfunction and as a protective measure in vocal warm-up, respectively. With improved biological data, our modeling framework has the capacity to transition from phenomenological to predictive, and may be a valuable tool in the exploration of the role of edema in voice disorders.

B. Modeling

This work employs a Bernoulli-based 1D flow model to capture glottal loading. While computationally efficient and adequate for bulk energy transfer (Decker and Thomson, 2007; Titze, 1988; Zhang, 2009), it cannot capture higher-order phenomena, such as entrance effects (Li *et al*., 2021; Zhang *et al*., 2020). Our acoustic treatment is likewise simplified: subglottal and supraglottal tracts are omitted, resonance is not modeled, and radiated pressure is estimated with a piston-in-baffle analogy. These simplifications mean that the acoustic results should be interpreted qualitatively. The primary contribution of this study is to demonstrate how long-time scale tissue processes (e.g., edema progression) can be coupled to voice production, and the modular framework readily accommodates higher-fidelity flow and acoustic models in future work.

Our model only captures compensatory adjustments through subglottal pressure, which is the primary factor governing vocal loudness. In practice, other adjustments, such as altering vocal tract resonance or laryngeal posturing, can also increase loudness. These strategies may lessen the predicted edema growth rate, since resonance adjustments are expected to contribute less to tissue trauma than pressure-driven loading. Compensations in other dimensions (e.g., pitch) could also influence outcomes, and might be modeled with VF posturing frameworks (Jiang *et al*., 2024; Vahabzadeh-Hagh *et al*., 2017) or, in simplified form, by varying tissue stiffness. However, the impact of such muscular adjustments on phonotrauma remains difficult to predict.

Our multi-time scale analysis assumes distinct tissue and voicing time scales, which is not always realistic. We considered a single nominal set of VF properties held constant during voicing, yet speakers adjust their habits, and thus tissue properties, across diverse time scales influenced by environment, personality, and activity. Likewise, we modeled phonotrauma as a gradual process on long tissue time scales, although acute trauma can also arise within short voicing time scales. These complexities blur the separation of time scales and may require more refined analyses.

Last, a full mesh convergence study for the long-time swelling simulations was not performed due to prohibitive computational cost. Pilot grid-independence checks indicated stable modal frequencies and mode shapes, suggesting the discretization is adequate; nevertheless, some residual numerical error cannot be excluded.

VI. CONCLUSION

This work presents the first-ever model for exploring the impact of VF swelling on phonation and, furthermore, to observe how swelling may progress in continued voice use as the vocal organ is modified by the influx of fluid. To the best of our knowledge, this is also the first model in voiced speech that incorporates both the short time scale tissue vibration and the long time scale tissue modification. Using this coupled model, we simulated edema progression over time for varying levels of damage sensitivity (the proportionality between edema and phonotrauma measure) and for two different mechanical measures of phonotrauma (viscous dissipation and positive strain energy rate). We also performed a growth rate analysis of the edema progression to gain insight into its governing factors.

Our model predicted that the progression of edema is non-homogeneous and that the growth rate of edema depends on the damage sensitivity (the sensitivity of edema to phonotrauma) relative to the effects of healing. When the inflammatory response is highly sensitive to phonotrauma and overcomes the rate at which healing promotes homeostasis, edema grows rapidly with time. We also found that the distribution of edema is non-homogeneous due to the non-uniformity of phonotrauma measures. Both viscous dissipation and strain energy rate resulted in edema concentrated near the medial surface (around contact) and within the VF body. These edema concentrations resulted in the development of medial surface bumps that altered the glottal airflow loading and necessitated compensatory subglottal pressure increases.

Clinically, our model supports the idea of a PVH "vicious cycle" that could result in self-reinforcing growth of edema which could eventually develop into phonotraumatic lesions. The model is particularly useful because it allows *in silico* exploration of the factors that control this growth. Development of phonotraumatic lesions is a complex process with numerous factors that affect whether or not they develop, ranging from personality to biomechanical differences (Hillman *et al.*, 2020). The model developed herein allows a systematic exploration of these factors through the model parameters; for example, through differences in VF properties, or the healing rate. This could aid in understanding the role of different factors in the etiology of PVH. More generally, our model could also be extended to explore remodeling of VF tissue and the development of nodules, which plays an important role in voice health. Nodule development involves fibrosis (Martins *et al.*, 2010), which would likely change tissue stiffness differently than the edema model considered here.

ACKNOWLEDGMENTS

Research reported in this publication was supported by the National Institute on Deafness and Other Communication Disorders of the National Institutes of Health Award No. P50DC015446. The authors thank Professor Preeti Sivasankar and Professor Nicole Li-Jessen for valuable insights on VF edema and comments on the manuscript.

AUTHOR DECLARATIONS

Conflict of Interest

The authors have no conflicts to disclose.

DATA AVAILABILITY

The data that support the findings of this study are available from the corresponding author upon reasonable request.

Alipour-Haghighi, F., Berry, D. A., and Titze, I. R. (**2000**). "A finite-element model of vocal-fold vibration," J. Acoust. Soc. Am. **108**(6), 3003–3012.

Balzani, D., Brinkhues, S., and Holzapfel, G. A. (**2012**). "Constitutive framework for the modeling of damage in collagenous soft tissues with application to arterial walls," Comput. Methods Appl. Mech. Eng. **213**, 139–151.

Bastian, R. W., Keidar, A., and Verdolini-Marston, K. (**1990**). "Simple vocal tasks for detecting vocal fold swelling," J. Voice **4**(2), 172–183.

Bonet, J., and Wood, R. D. (**2008**). *Nonlinear Continuum Mechanics for Finite Element Analysis*, 2nd ed. (Cambridge University Press, London, UK).

Branski, R. C., Barbieri, S. S., Weksler, B. B., Saltman, B., Verdolini Abbott, K. V., and Rosen, C. A. (**2009**). "Effects of transforming growth factor-β1 on human vocal fold fibroblasts," Ann. Otol. Rhinol. Laryngol. **118**(3), 218–226.

Chaboche, J. L. (**1988**). "Continuum damage mechanics: I. General concepts," J. Appl. Mech. **55**(1), 59–64.

Chhetri, D. K., and Park, S. J. (**2016**). "Interactions of subglottal pressure and neuromuscular activation on fundamental frequency and intensity," Laryngoscope **126**(5), 1123–1130.

Czerwonka, L., Jiang, J. J., and Tao, C. (**2008**). "Vocal nodules and edema may be due to vibration-induced rises in capillary pressure," Laryngoscope **118**(4), 748–752.

Decker, G. Z., and Thomson, S. L. (**2007**). "Computational simulations of vocal fold vibration: Bernoulli versus Navier–Stokes," J. Voice **21**(3), 273–284.

Deng, J. J., Erath, B. D., Zañartu, M., and Peterson, S. D. (**2023**). "The effect of swelling on vocal fold kinematics and dynamics," Biomech. Model. Mechanobiol. **22**(6), 1873–1889.

Deng, J. J., and Peterson, S. D. (**2023**). "Examining the influence of epithelium layer modeling approaches on vocal fold kinematics and kinetics," Biomech. Model. Mechanobiol. **22**(2), 479–493.

Galindo, G. E., Peterson, S. D., Erath, B. D., Castro, C., Hillman, R. E., and Zañartu, M. (**2017**). "Modeling the pathophysiology of phonotraumatic vocal hyperfunction with a triangular glottal model of the vocal folds," J. Speech Lang. Hear. Res. **60**(9), 2452–2471.
Geng, B., Movahhedi, M., Xue, Q., and Zheng, X. (**2021**). "Vocal fold vibration mode changes due to cricothyroid and thyroarytenoid muscle interaction in a three-dimensional model of the canine larynx," J. Acoust. Soc. Am. **150**(2), 1176–1187.
Gordon Betts, J., Desaix, P., Johnson, E., Johson, J. E., Korol, O., Kruse, D., Poe, B., Wise, J. A., Womble, M., and Young, K. A. (**2022**). *Anatomy and Physiology 2e*, 2nd ed. (OpenStax, Houston, TX).
Gou, K., and Pence, T. J. (**2016**). "Hyperelastic modeling of swelling in fibrous soft tissue with application to tracheal angioedema," J. Math. Biol. **72**(1), 499–526.
Gunter, H. E. (**2004**). "Modeling mechanical stresses as a factor in the etiology of benign vocal fold lesions," J. Biomech. **37**(7), 1119–1124.
Gurtin, M. E., Fried, E., and Anand, L. (**2010**). *The Mechanics and Thermodynamics of Continua* (Cambridge University Press, London, UK).
Haben, C. M. (**2012**). "Voice rest and phonotrauma in singers," Med. Probl. Perform. Artists **27**, 165–168.
Hansbo, P., and Larson, M. G. (**2014**). "Finite element modeling of a linear membrane shell problem using tangential differential calculus," Comput. Methods Appl. Mech. Eng. **270**, 1–14.
Harris, C. R., Millman, K. J., van der Walt, S. J., Gommers, R., Virtanen, P., Cournapeau, D., Wieser, E., Taylor, J., Berg, S., Smith, N. J., Kern, R., Picus, M., Hoyer, S., van Kerkwijk, M. H., Brett, M., Haldane, A., del Río, J. F., Wiebe, M., Peterson, P., Gérard-Marchant, P., Sheppard, K., Reddy, T., Weckesser, W., Abbasi, H., Gohlke, C., and Oliphant, T. E. (**2020**). "Array programming with NumPy," Nature **585**(7825), 357–362.
Hillman, R. E., Stepp, C. E., Van Stan, J. H., Zañartu, M., and Mehta, D. D. (**2020**). "An updated theoretical framework for vocal hyperfunction," Am. J. Speech Lang. Pathol. **29**(4), 2254–2260.
Hirano, M., and Kakita, Y. (**1985**). "Cover-body theory of vocal fold vibration," in *Speech Science Recent Advances*, edited by R. Daniloff (College-Hill Press, San Diego, CA), pp. 1–46.
Hirano, M., Kakita, Y., Ohmaru, K., and Kurita, S. (**1982**). "Structure and mechanical properties of the vocal fold," Speech Lang. **7**(4), 271–297.
Holmberg, E. B., Doyle, P., Perkell, J. S., Hammarberg, B., and Hillman, R. E. (**2003**). "Aerodynamic and acoustic voice measurements of patients with vocal nodules: Variation in baseline and changes across voice therapy," J. Voice **17**(3), 269–282.
Hortobagyi, D., Grossmann, T., Tschernitz, M., Grill, M., Kirsch, A., Gerstenberger, C., and Gugatschka, M. (**2020**). "*In vitro* mechanical vibration down-regulates pro-inflammatory and pro-fibrotic signaling in human vocal fold fibroblasts," PLoS One **15**(11), e0241901.
Hunter, E. J., and Titze, I. R. (**2009**). "Quantifying vocal fatigue recovery: Dynamic vocal recovery trajectories after a vocal loading exercise," Ann. Otol. Rhinol. Laryngol. **118**(6), 449–460.
Ingle, J. W., Helou, L. B., Li, N. Y. K., Hebda, P. A., Rosen, C. A., and Verdolini Abbott, K. V. (**2014**). "Role of steroids in acute phonotrauma: A basic science investigation," Laryngoscope **124**(4), 921–927.
Jiang, J. J., Chen, H.-J., Stern, J., and Solomon, N. P. (**2004**). "Vocal efficiency measurements in subjects with vocal polyps and nodules: A preliminary report," Ann. Otol. Rhinol. Laryngol. **113**(4), 277–282.
Jiang, J. J., and Titze, I. R. (**1994**). "Measurement of vocal fold intraglottal pressure and impact stress," J. Voice **8**(2), 132–144.
Jiang, W., Geng, B., Zheng, X., and Xue, Q. (**2024**). "A computational study of the influence of thyroarytenoid and cricothyroid muscle interaction on vocal fold dynamics in an MRI-based human laryngeal model," Biomech. Model. Mechanobiol. **23**(5), 1801–1813.
Johns, M. M. (**2003**). "Update on the etiology, diagnosis, and treatment of vocal fold nodules, polyps, and cysts," Curr. Opin. Otolaryngol. Head Neck Surg. **11**(6), 456–461.
Kinsler, L. E., Frey, A. R., Coppens, A. B., and Sanders, J. V. (**2000**). *Fundamentals of Acoustics*, 4th ed. (John Wiley & Sons, New York).
Leydon, C., Imaizumi, M., Bartlett, R. S., Wang, S. F., and Thibeault, S. L. (**2014**). "Epithelial cells are active participants in vocal fold wound healing: An *in vivo* animal model of injury," PLoS One **9**(12), e115389.
Li, Z., Chen, Y., Rousseau, B., and Luo, H. (**2021**). "A one-dimensional flow model enhanced by machine learning for simulation of vocal fold vibration," J. Acoust. Soc. Am. **149**(3), 1712–1723.
Logg, A., and Wells, G. N. (**2010**). "DOLFIN," ACM Trans. Math. Softw. **37**(2), 1–28.
Martins, R. H. G., Defaveri, J., Custódio Domingues, M. A., De Albuquerque e Silva, R., and Fabro, A. (**2010**). "Vocal fold nodules: Morphological and immunohistochemical investigations," J. Voice **24**(5), 531–539.
Miri, A. K. (**2014**). "Mechanical characterization of vocal fold tissue: A review study," J. Voice **28**(6), 657–667.
Mortimer, P. S., and Levick, J. R. (**2004**). "Chronic peripheral oedema: The critical role of the lymphatic system," Clin. Med. J. R. Coll. Phys. Lond. **4**(5), 448–453.
Motie-Shirazi, M., Zañartu, M., Peterson, S. D., and Erath, B. D. (**2021**). "Vocal fold dynamics in a synthetic self-oscillating model: Contact pressure and dissipated-energy dose," J. Acoust. Soc. Am. **150**(1), 478–489.
Motie-Shirazi, M., Zañartu, M., Peterson, S. D., Mehta, D. D., Hillman, R. E., and Erath, B. D. (**2023**). "Effect of nodule size and stiffness on phonation threshold and collision pressures in a synthetic hemilaryngeal vocal fold model," J. Acoust. Soc. Am. **153**(1), 654–664.
Murphy Estes, C., Chadwick, K., Sadoughi, B., Andreadis, K., Sussman, S., and Sulica, L. (**2022**). "Performers' perceptions of vocal function during oral steroid treatment of vocal fold edema," Laryngoscope **132**(12), 2434–2441.
Murray, P. R., and Thomson, S. L. (**2011**). "Synthetic, multi-layer, self-oscillating vocal fold model fabrication," J. Vis. Exp. **58**, e3498.
Newmark, N. M. (**1962**). "A method of computation for structural dynamics," Trans. Am. Soc. Civ. Eng. **127**(1), 1406–1433.
Nudelman, C. J., Ortiz, A. J., Fox, A. B., Mehta, D. D., Hillman, R. E., and Van Stan, J. H. (**2022**). "Daily phonotrauma index: An objective indicator of large differences in self-reported vocal status in the daily life of females with phonotraumatic vocal hyperfunction," Am. J. Speech Lang. Pathol. **31**(3), 1412–1423.
Pavliotis, G. A., and Stuart, A. M. (**2008**). *Multiscale Methods: Texts Applied in Mathematics* (Springer, New York), Vol. 53.
Pence, T. J., and Tsai, H. (**2005**). "On the cavitation of a swollen compressible sphere in finite elasticity," Int. J. Non. Linear Mech. **40**(2), 307–321.
Rousseau, B., Sohn, J., Tateya, I., Montequin, D. W., and Bless, D. M. (**2004**). "Functional outcomes of reduced hyaluronan in acute vocal fold scar," Ann. Otol. Rhinol. Laryngol. **113**(10), 767–776.
Scherer, R. C., Shinwari, D., De Witt, K. J., Zhang, C., Kucinschi, B. R., and Afjeh, A. A. (**2001**). "Intraglottal pressure profiles for a symmetric and oblique glottis with a divergence angle of 10 degrees," J. Acoust. Soc. Am. **109**(4), 1616–1630.
Tao, C., and Jiang, J. J. (**2007**). "Mechanical stress during phonation in a self-oscillating finite-element vocal fold model," J. Biomech. **40**(10), 2191–2198.
Titze, I. R. (**1988**). "The physics of small-amplitude oscillation of the vocal folds," J. Acoust. Soc. Am. **83**(4), 1536–1552.
Titze, I. R., and Hunter, E. J. (**2015**). "Comparison of vocal vibration-dose measures for potential-damage risk criteria," J. Speech. Lang. Hear. Res. **58**(5), 1425–1439.
Tsai, H., Pence, T. J., and Kirkinis, E. (**2004**). "Swelling induced finite strain flexure in a rectangular block of an isotropic elastic material," J. Elast. **75**(1), 69–89.
Vahabzadeh-Hagh, A. M., Zhang, Z., and Chhetri, D. K. (**2017**). "Three-dimensional posture changes of the vocal fold from paired intrinsic laryngeal muscles," Laryngoscope **127**(3), 656–664.
Verdolini, K., Rosen, C. A., Branski, R. C., and Hebda, P. A. (**2003**). "Shifts in biochemical markers associated with wound healing in laryngeal secretions following phonotrauma: A preliminary study," Ann. Otol. Rhinol. Laryngol. **112**(12), 1021–1025.
Verdolini Abbott, K., Li, N. Y., Branski, R. C., Rosen, C. A., Grillo, E., Steinhauer, K., and Hebda, P. A. (**2012**). "Vocal exercise may attenuate acute vocal fold inflammation," J. Voice **26**(6), 814.e1–814.e13.
Virtanen, P., Gommers, R., Oliphant, T. E., Haberland, M., Reddy, T., Cournapeau, D., Burovski, E., Peterson, P., Weckesser, W., Bright, J., van der Walt, S. J., Brett, M., Wilson, J., Millman, K. J., Mayorov, N., Nelson, A. R., Jones, E., Kern, R., Larson, E., Carey, C. J., Polat, I., Feng, Y., Moore, E. W., VanderPlas, J., Laxalde, D., Perktold, J., Cimrman, R., Henriksen, I., Quintero, E. A., Harris, C. R., Archibald, A. M., Ribeiro, A. H., Pedregosa, F., van Mulbregt, P., Vijaykumar, A., Bardelli, A. P., Rothberg, A., Hilboll, A., Kloeckner, A., Scopatz, A., Lee, A., Rokem,

A., Woods, C. N., Fulton, C., Masson, C., Häggström, C., Fitzgerald, C., Nicholson, D. A., Hagen, D. R., Pasechnik, D. V., Olivetti, E., Martin, E., Wieser, E., Silva, F., Lenders, F., Wilhelm, F., Young, G., Price, G. A., Ingold, G. L., Allen, G. E., Lee, G. R., Audren, H., Probst, I., Dietrich, J. P., Silterra, J., Webber, J. T., Slavič, J., Nothman, J., Buchner, J., Kulick, J., Schönberger, J. L., de Miranda Cardoso, J. V., Reimer, J., Harrington, J., Rodríguez, J. L. C., Nunez-Iglesias, J., Kuczynski, J., Tritz, K., Thoma, M., Newville, M., Kümmerer, M., Bolingbroke, M., Tartre, M., Pak, M., Smith, N. J., Nowaczyk, N., Shebanov, N., Pavlyk, O., Brodtkorb, P. A., Lee, P., McGibbon, R. T., Feldbauer, R., Lewis, S., Tygier, S., Sievert, S., Vigna, S., Peterson, S., More, S., Pudlik, T., Oshima, T., Pingel, T. J., Robitaille, T. P., Spura, T., Jones, T. R., Cera, T., Leslie, T., Zito, T., Krauss, T., Upadhyay, U., Halchenko, Y. O., and Vázquez-Baeza, Y. (**2020**). "SciPy 1.0: Fundamental algorithms for scientific computing in Python," Nat. Methods **17**(3), 261–272.

Watson, K., Oates, J., Sinclair, C., Smith, J. A., and Phyland, D. (**2024**). "Associations between immunological biomarkers, voice use patterns, and phonotraumatic vocal fold lesions: A scoping review," J. Voice. (published online).

Yang, S., Zhang, Y., Mills, R. D., and Jiang, J. J. (**2017**). "Quantitative study of the effects of dehydration on the viscoelastic parameters in the vocal fold mucosa," J. Voice **31**(3), 269–274.

Zhang, Y., Zheng, X., and Xue, Q. (**2020**). "A deep neural network based glottal flow model for predicting fluid-structure interactions during voice production," Appl. Sci **10**(2), 705.

Zhang, Z. (**2009**). "Characteristics of phonation onset in a two-layer vocal fold model," J. Acoust. Soc. Am. **125**(2), 1091–1102.

Zhuang, P., Sprecher, A. J., Hoffman, M. R., Zhang, Y., Fourakis, M., Jiang, J. J., and Wei, C. S. (**2009**). "Phonation threshold flow measurements in normal and pathological phonation," Laryngoscope **119**(4), 811–815.